UNIAXIAL TENSILE PROPERTIES OF AS4 3D WOVEN COMPOSITES WITH FOUR DIFFERENT RESIN SYSTEMS: EXPERIMENTAL RESULTS AND ANALYSIS – PROPERTY COMPUTATIONS

Babak Farrokh[1], Kenneth N. Segal[1], Trenton M. Ricks[2], Sandi G. Miller[2], Benjamin T. Rodini[3], and David S. Sleight[4]

[1] NASA Goddard Space Flight Center, 8800 Greenbelt Rd, Greenbelt, MD, 20771
[2] NASA Glenn Research Center, 21000 Brookpark Road, Cleveland, OH 44135
[3] ATA Aerospace LLC, 7474 Greenway Center Drive, Greenbelt, MD 20770
[4] NASA Langley Research Center, 1 NASA Drive, Hampton, VA 23666

ABSTRACT

As a part of the NASA Composite Technology for Exploration project, eight different AS4 3D orthogonal woven composite panels were manufactured and were subjected to mechanical testing including uniaxial tension along the weaves' warp direction. Each set, with four different resin systems (KCR-IR6070, EP2400, RTM6, and RS-50), included weave architectures designed using 12K and 6K AS4 carbon fiber yarns. For the tension testing conducted at Room Temperature Ambient (RTA) condition, the elastic modulus and strength of these eight panels (as-processed and thermally cycled) were measured and compared while the potential evolution of micro-cracking before and after thermal cycling were monitored via optical microscopy and X-Ray Computed Tomography. The data set also included test results of the as-processed materials at Elevated Temperature Wet (ETW) condition. In the second part of this study, efforts were made to compute elastic constants for AS4 6K/RTM6 and AS4 12K/RTM6 materials by implementing a finite element approach and the Multiscale Generalized Method of Cells (MSGMC) technique developed at NASA Glenn Research Center. Digimat-FE was used to model the weave architectures, assign properties, calculate yarn properties, create the finite element mesh, and compute the elastic properties by applying periodic boundary conditions to finite element models of each repeating unit cell. The required input data for MSGMC was generated using Matlab® from Digimat exported weave information. Experimental and computational results were compared, and the differences and limitations in correlating to the test data were briefly discussed.

1. INTRODUCTION

1.1 Background

The NASA Composite Technology for Exploration (CTE) project has been involved with the development of composite technologies and, in particular, is aimed to further advance the state-of-the-art in areas related to *bonded joints technology* in inclusive areas of design, manufacturing, analysis, testing, and test-correlation. The CTE project has been demonstrating

through case studies that, the applications of *composite bonded joints* in heavy lift launch vehicles, can reduce the mass and part counts by around 50% and 80%, respectively, as compared with their metallic bolted counterparts.

For this purpose and along with the process of trading different composite joint materials and configurations, 3D woven composites were considered for evaluations. 3D woven composites have been identified to offer good potentials in circumferential joints and end fittings applications due to their enhanced performance (*e.g.*, delamination resistance) and the possibility of being woven in curved section along with their damage tolerance and fatigue resistance [1]. With all these advantages over traditional 2D laminates, 3D woven composites are known to exhibit significant micro-cracking. This is mainly due to the existence of through the thickness carbon yarns and hence additional constraint in the thickness direction. The extra constraint along with a relatively large *coefficient of thermal expansion* mismatch between the carbon fiber and resin can develop higher triaxial stresses which result in micro-crack formation within the material (generally in resin pockets) during the cool down in the curing process [2]. Therefore, it is crucial to understand the influence and evolution of this phenomenon on material performance and through the life of 3D woven composite parts and to investigate ways in which the micro-cracking could be avoided.

1.2 Objectives

One of the objectives of this work was to study the evolution of micro-cracking as functions of four different resin systems (toughened and un-toughened epoxies), finer (6K) versus coarser (12K) fiber yarns, and thermal cycling after processing and to explore how these parameters could influence the mechanical properties and performance (in particular, uniaxial tensile response) of such material systems. As an added value study and to take an advantage of the collected test data, as our secondary objective, the weave architectures were modeled and elastic properties of were computed using a finite element (FE)-based approach and a semi-analytical technique, and results were compared with experimental data.

2. MATERIALS, PROCESSES, AND WEAVE ARCHITECTURES

2.1 Materials and Processes

An AS4 carbon fiber[1] with two different tow sizes (6K and 12K) along with four different resin systems (KCR-IR6070, EP2400, RTM6, and RS-50) were selected for this study. The combinations resulted in eight flat 63.5 cm by 63.5 cm (3.175 mm thick) panels which were first woven and then resin infused by Bally Ribbon Mills (BRM), Inc. and North Coast Companies, Inc., respectively. A summary of the fabricated panels is provided in Table 1.

To investigate the influence of thermal cycling on micro-crack density and hence any potential effects on mechanical properties, a series of test coupons (to be explained later) were cut from each panel and subjected to thermal cycling between -55 ºC to 80 ºC for 400 cycles (an 18 day process, ~ 1 hour per cycle).

[1] The use of trademarks or names of manufacturers in this report is for accurate reporting and does not constitute an official endorsement, either expressed or implied, of such products or manufacturers by the National Aeronautics and Space Administration.

Table 1. Material systems with designated names and panel serial numbers.

SN#	Fiber Material	Tow Size	Resin System	Panel /Material Designation
SN001	AS4	6K	KCR-IR6070	AS4 6K/KCR-IR6070
SN002		12K		AS4 12K/KCR-IR6070
SN003		6K	EP2400	AS4 6K/EP2400
SN004		12K		AS4 12K/EP2400
SN005		6K	RTM6	AS4 6K/RTM6
SN006		12K		AS4 12K/RTM6
SN007		6K	RS-50	AS4 6K/RS-50
SN008		12K		AS4 12K/RS-50

2.2 Weave Architecture

Two weave configurations were designed by BRM. The weaves were of the 3D orthogonal type with 1-Z yarn per dent arrangement. The Repeating Unit Cells (RUCs) of these weave architectures are shown in Figure 1. More details on the weave parameters, number of layers, directional percentage fiber, and fiber volume fraction, can be found in Table 2. It should be noted that, the directional percentage fiber and fiber volume are the actual measurements, by BRM, on the dry woven product (based on an assumed nominal panel thickness of 3.175 mm) and not the calculated values.

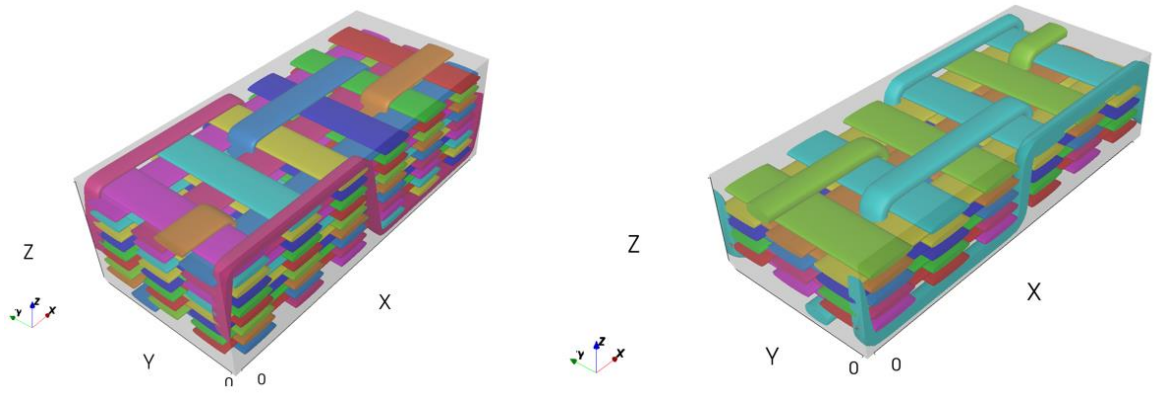

Figure 1. TexGen [3] illustration of weave RUC architectures by BRM; Left: 6K, and Right: 12K configurations.

Table 2. 3D orthogonal weave parameters; 6K and 12K configurations.

Configuration	Fiber	Per Layer		# of Warp Layers	# of Weft Layers	Unit Cell Dims *mm*	% Fiber Fraction			% Fiber Volume	Z Fiber per Dent
		Warp Yarns Per *cm*	Weft Yarns Per *cm*				WARP	WEFT	Z		
1	AS4-6K	3.93	3.54	8	9	16.8 x 7.6 x 3.2	46.6	46.6	7.3	50.9	1
2	AS4-12K	3.54	3.14	4	5	19.1 x 8.5 x 3.2	41	46.4	12.6	52.6	1

3. MATERIALS CHARACTERIZATIONS AND MECHANICAL TESTING

3.1 Materials Characterization

Fiber volume fraction, V_f, and void content were measured, at NASA Glenn Research Center (GRC), according to ASTM D3171 on four sample replicates on each panel prior to any thermal cycling. To evaluate the extent of micro-cracking before and after thermal cycling optical microscopy (at NASA GRC) and X-Ray Computed Tomography (CT) (at NASA Goddard Space Flight center (GSFC)) were performed, and the resulting images were compared.

3.2 Mechanical Testing

A series of mechanical testing, in the warp direction, were performed at Room Temperature Ambient (RTA) on the as-processed (AP) and thermally cycled (TC) materials as well as coupons that were tested at Elevated Temperature Wet (ETW) on the AP material systems. The testing included tension (ASTM D3039), compression (ASTM D6641), short beam shear (ASTM D2344), and single shear bearing (ASTM D5691). All panels were cut, thermal cycled, instrumented, and tested by the National Institute for Aviation Research (NIAR).

3.2.1 Instrumentation

In order to accurately measure strain in the test, the following instrumentations were utilized:

- Tension: RTA – Metal foil strain gages (all coupons) and Digital Image Correlation (DIC) on only two samples per material. ETW – Metal foil strain gage and extensometer (all coupons).
- Compression: RTA and ETW – Extensometer (all coupons)
- Single shear bearing: RTA – Extensometer (all coupons) and DIC on only two samples per material.
- Short beam shear: None

4. EXPERIMENGTAL RESULTS AND DISCUSSION

4.1 Materials Characterization

4.1.1 Fiber volume fraction and void content

Table 3 shows the results from acid digestion measurements (ASTM D3171) indicating the fiber V_f and void content for all eight panels in the AP condition. No measurements were conducted on TC materials. The relatively low standard deviations in measurements suggests uniform fiber volume fraction and void content throughout the panels as the four samples were arbitrarily cut from four different locations on each panel.

As indicated in Table 2, BRM calculated the fiber volume fraction of the 6K and 12K weave architectures to be 50.9% and 52.6%, respectively. This calculation was based on measuring the dry weave fiber weights and assuming a nominal (3.175 mm) thickness for all panels. The actual fiber volume measurements, as shown in Table 3, were somewhat different. However, a trend of V_f (12K) > V_f (6K) was observed for all measurements including those calculated by BRM. The differences between the BRM reported values and measurements were anticipated to mainly arise from the variations between the nominal and as-built panel thicknesses. Thickness

measurements on the eight panels showed slightly larger thicknesses ranging from 3.175 mm (nominal) to 3.327 mm.

Table 3. ASTM D3171 measurement results for all eight panels: V_f and void content.

Panel	Resin	% Void Content		% Fiber Volume	
		Avg.	SD	Avg.	SD
SN001	KCR-IR6070	~ 0	0.2	47.3	0.3
SN002		~ 0	0.4	50.6	0.8
SN003	EP2400	1.4	0.2	49.7	0.5
SN004		1.1	0.4	51.5	0.9
SN005	RTM6	0.4	0.3	47.4	0.3
SN006		~ 0	0.5	48.4	1.2
SN007	RS-50	1.1	0.2	47.3	0.6
SN008		1.2	0.1	48.6	0.9

4.1.2 Micro-cracking assessment (optical microscopy and X-ray CT)

The images from optical microscopy revealed that micro-cracks developed in all panels, likely, during the curing process and cool down, regardless of resin type (toughened, KCR-IR6070 and EP2400; or un-toughened, RTM6 and RS-50) or fiber tow size. Generally, micro-cracking was observed near the Z-fibers. The density of micro-cracks was clearly increased as materials underwent thermal cycling and, in addition to Z-fiber ends, cracks were distributed further within the woven composites, including individual fiber tows. At this point, no conclusions can be drawn as which material system exhibited less (or more) micro-cracking. Developing an imaging technique to measure the cumulative volumes of the micro-cracks within these samples is an ongoing work at NASA GSFC. Figure 2 shows a few representative optical microscopy images for the AP and TC for SN001 and SN006 with some micro-cracks labeled using yellow arrows.

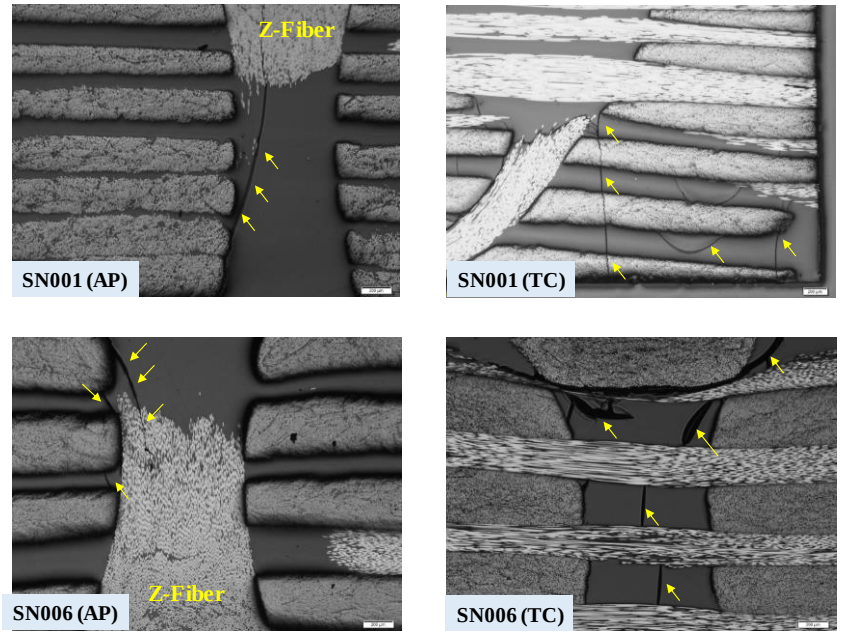

Figure 2. Optical microscopy images illustrating the extent of micro-cracks in SN001 (with toughened epoxy) and SN006 (with un-toughened epoxy) before and after thermal cycling.

The assessment obtained by inspecting optical microscopy images were further confirmed by reviewing the results from X-Ray CT. Figures 3-4 and Figures 5-6 show the X-Ray CT images in two perpendicular cross-sections for SN001 and SN006 for the AP and CT materials, respectively. It is evident that the thermal cycling introduced more cracks into the composite. There were cracks through resin rich areas as well as cracks that were extended through the fiber tows.

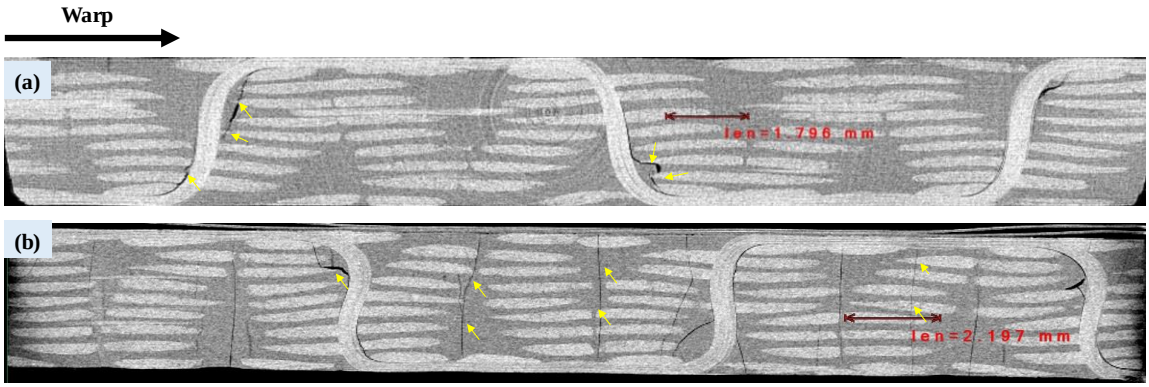

Figure 3. X-Ray CT images of Warp-Z plane cross-section for SN001 a) AP and b) TC material.

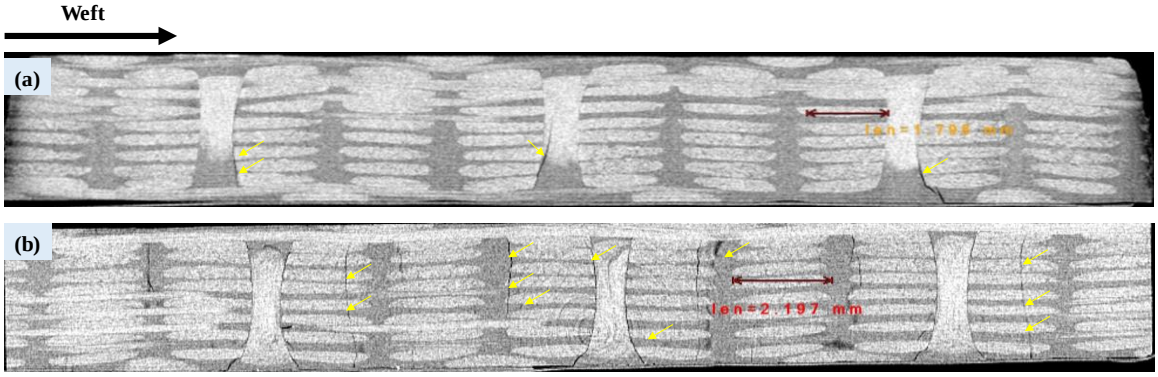

Figure 4. X-Ray CT images of Weft-Z plane cross-section for SN001 a) AP and b) TC material.

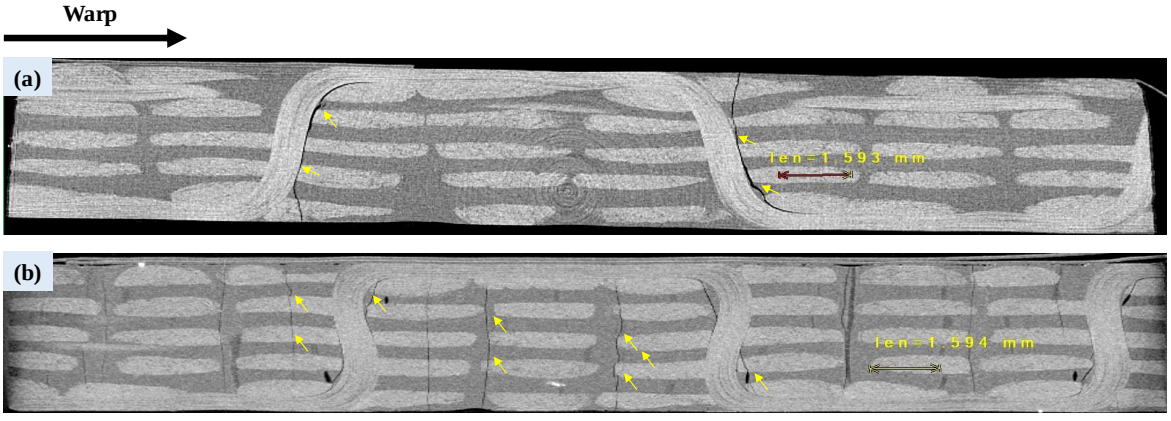

Figure 5. X-Ray CT images of Warp-Z plane cross-section for SN006 a) AP and b) TC material.

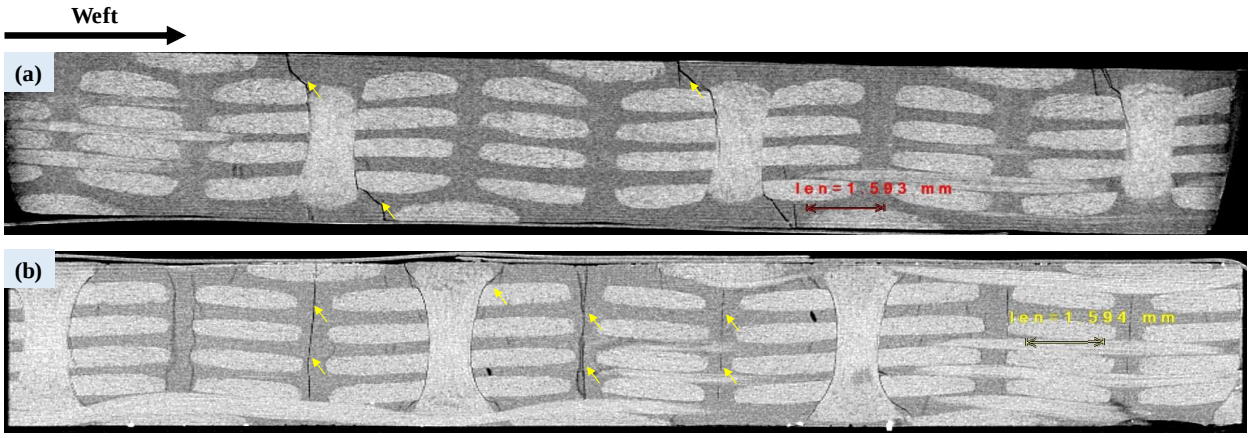

Figure 6. X-Ray CT images of Weft-Z plane cross-section for SN006 a) AP and b) TC material.

4.2 Mechanical Testing

4.2.1 Tensile Testing

AP and CP coupons for RTA testing were instrumented with strain gages while DIC was also used for each set, on two (out of five) specimens. On AP coupons for ETW testing, strain gages were used and each coupon was further instrumented with an extensometer for the strain measurement at the beginning of each test. Strain gages, generally, did not survive up to the failure strains; however, they all sufficiently functioned to strain levels, and beyond, necessary to accurately measuring the elastic modulus.

Figure 7 shows the RTA stress-strain responses (from DIC) of all eight panels for (a) AP and (b) TC conditions. The full stress-strain curves for each panel and conditions were limited to only two replicates per test since, as mentioned, DIC was only used on two (out of five) specimens and the strain gages generally did not survive to failure. The strains were measured by defining a virtual extensometer with the gage length of 7.6 cm (embedded sketch of Figure 7) to average the axial strain over a larger length (*i.e.*, over more RUCs). All coupons responded linearly to failure strains and generally a minimum strain to failure of ~12,000με was obtained for all the material systems. Overall, the 6K weave configuration showed slightly higher stiffness and strength, as expected, due to a tighter and finer weave structure and more layers existing in the given nominal thickness of 3.175 mm. The thermal cycling (*i.e.*, higher micro-crack density) although slightly affected the slope of the stress-statin curve, did not significantly influence the moduli or strength values, as the tests were performed in the warp yarn dominated direction. Therefore, as expected, the choice of resin systems and ETW condition had relatively minimal effects on the tensile performance of these four material systems. For a more quantitative comparison, the average modulus values (with standard deviation error bars using strain gage strains) and strength values are shown in the bar charts of Figures 8a and 8b, respectively, for RTA (AP), RTA (TC), and ETW (AP) conditions.

Higher standard deviations in elastic moduli (Figure 8a) were attributed to strain measurements using strain gages. A relatively small surface area of the gage grid (~9 mm x ~5 mm) together with larger unit cell size of these weave architectures (Table 2) could potentially cause such variations. This was further verified once the moduli of the ETW (AP) coupons measured by

both strain gages (~9 mm gage length) and extensometers (25.4 mm gage length) were compared side by side, as shown in Figure 9. For all panels, less variability in the tensile moduli was present in the extensometer data than those measured by the strain gages.

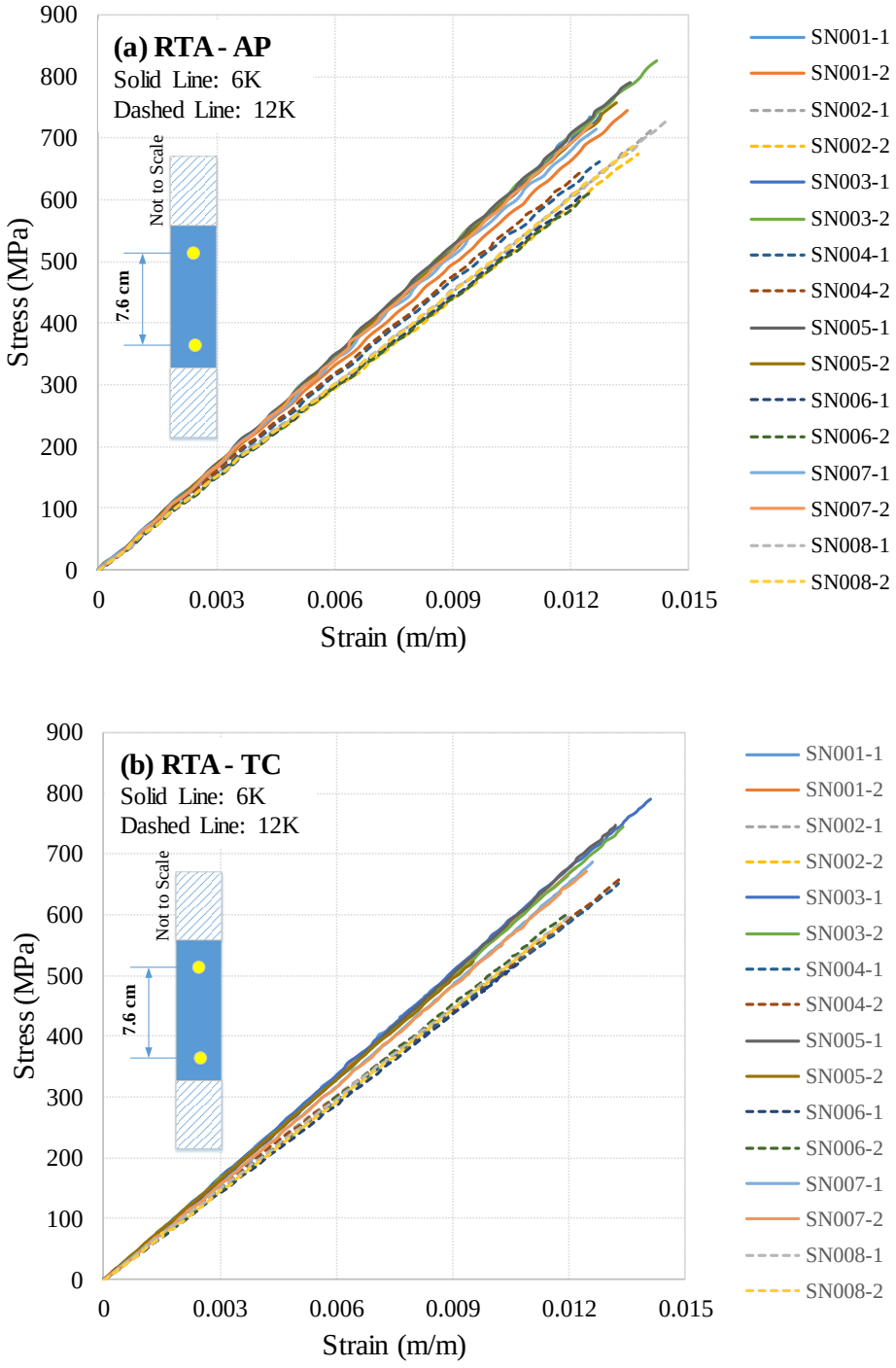

Figure 7. RTA Tensile stress-strain response of SN001-SN008 (from DIC) for a) AP and b) TC coupons.

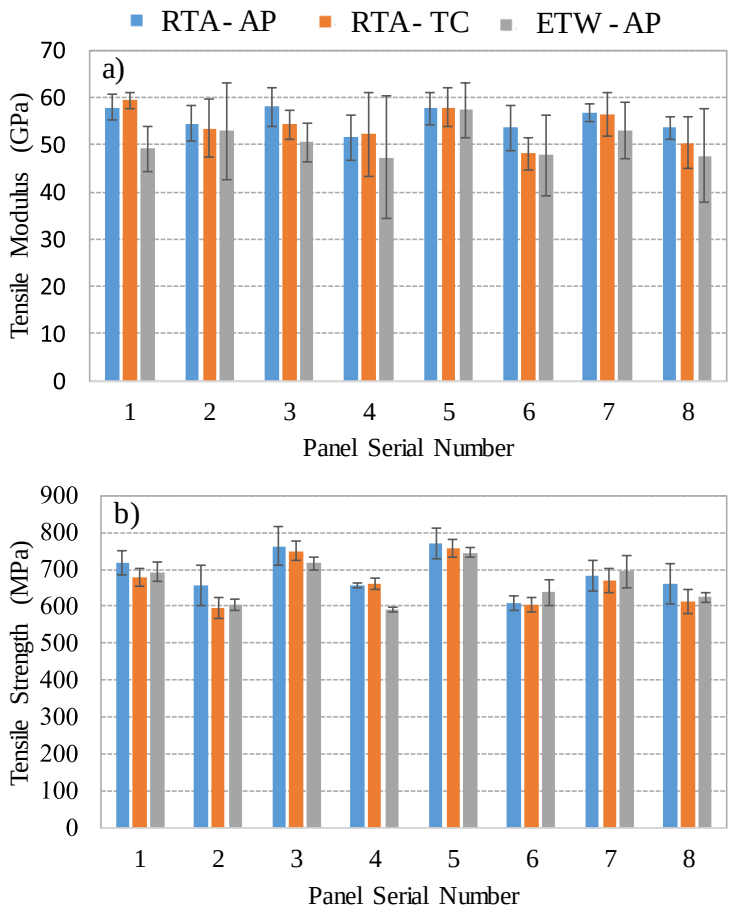

Figure 8. Tensile modulus from strain gages (a) and strength (b) values for RTA (AP,) RTA (TC), and ETW (AP).

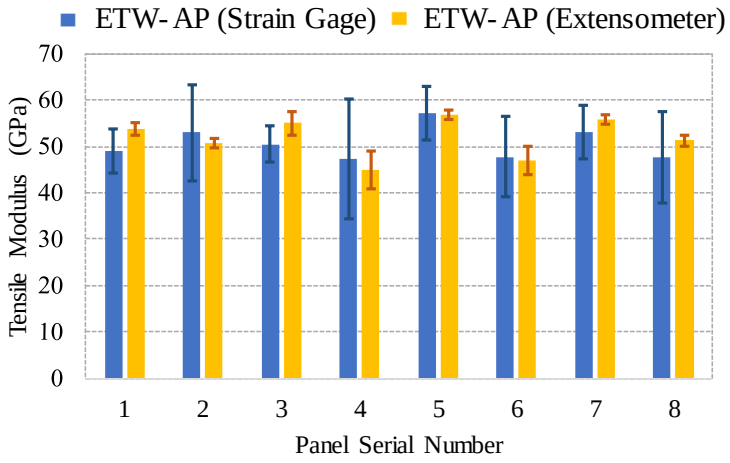

Figure 9. The ETW (AP) tensile modulus values from strain gage (blue) and extensometer (yellow).

4.2.2 Other (Non-Tensile) Testing

Figure 10 shows a summary of strength values obtained from compression, short beam shear, and bearing testing. The compressive strength values, as compared with the tensile counterparts, were around 50% lower, and in those although the 6K configuration always performed better, the ETW strength values were much lower than RTAs. A reason for this is that the resin loses stiffness at elevated temperature and cannot stabilize the warp yarns under compressive loads as it does at RTA.

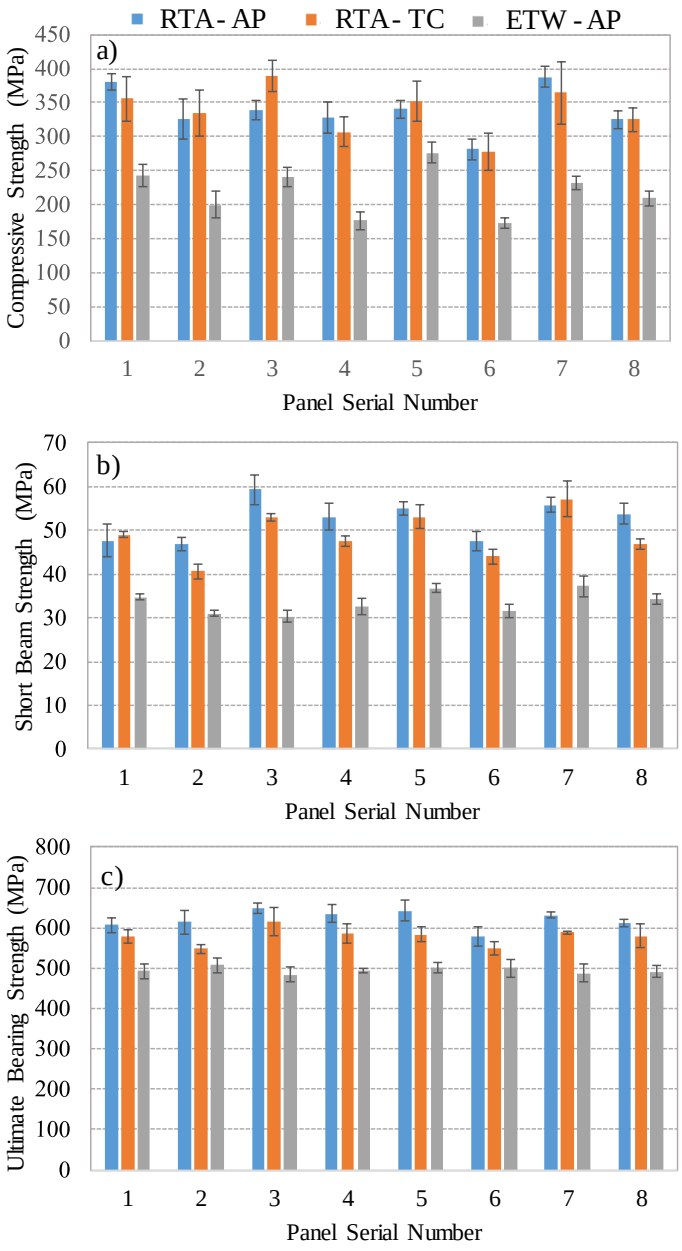

Figure 10. Strength values obtained from a) compression, b) short beam shear, and c) single lap shear bearing testing for RTA (AP), RTA (TC) and ETW (AP).

Additionally, the higher standard deviations in compressive strength is anticipated to raise from narrower (12.7 mm) coupon geometry in ASTM D6641 versus ASTM D3039 (25.4 mm wide specimen) as it is, again, related to a relatively large unit cell sizes in these weave architectures.

5. MATERIAL MODELING AND MECHANICAL PROPERTY PREDICTIONS

5.1 Approach

As mentioned, the eight fabricated panels were comprised of two weave architectures with four resin systems. The AS4/RTM6 material system was selected for modeling and analysis purposes of this study. Both 6K and 12K configurations were considered and the properties were computed and compared with the corresponding test data (*i.e.*, warp direction tensile modulus). In this regard, two different approaches were employed for the analysis and for computing the elastic properties of the AS4 (6K)/ RTM6 and AS4 (12K)/RTM6: Finite Element (FE) based approach and Multiscale Generalized Method of Cells (MSGMC).

5.1.1 Finite element (FE) based approach

FE approaches are commonly used to compute effective properties of (non-laminated) composites by FE modeling and analyzing an RUC mesh under relevant loads and boundary conditions. In this work, Digimat-FE Modeler and Digimat-FE Solver [4] were used as the material modeling platform and FE solver, respectively.

5.1.1.1 Digimat FE modeling process

Using the weave parameters (Table 2) and design illustrations (Figure 1) provided by BRM, Digimat-FE Modeler was used to model the two weave architectures, calculate yarn material properties, create the RUC geometries and FE meshes, and apply relevant loading and boundary conditions to calculate effective material properties. The 6K and 12K architectures were modeled with 1,368,000 and 1,147,500 hexahedral 8-noded elements, respectively. The 6K configuration is a finer weave so to achieve the same fidelity in the analysis, a finer FE mesh should be adapted for the 6K model as compared the 12K weave configuration. Figure 11 illustrates some of the modeling steps for both 6K and 12K architectures.

It should be mentioned here that, the design tool assumes perfect yarn geometries with constant cross sections throughout the materials' RUC. This is, however, somewhat different from the as-woven product as in real life the fiber yarns are *fighting for space* and thus, the presence of irregularities in the weave patterns and yarn cross-sections are unavoidable; something that currently cannot be captured in our modeling and analysis. Nevertheless, in order to achieve the intended RUC sizes and targeted fiber volume fractions, the filament counts in the Z-fibers were artificially reduced in the models; but in return, the axial moduli assigned to those Z-fibers were increased to achieve equivalent (to 12K or 6K) yarn axial stiffness values in order to compensate for the adopted smaller Z-yarns.

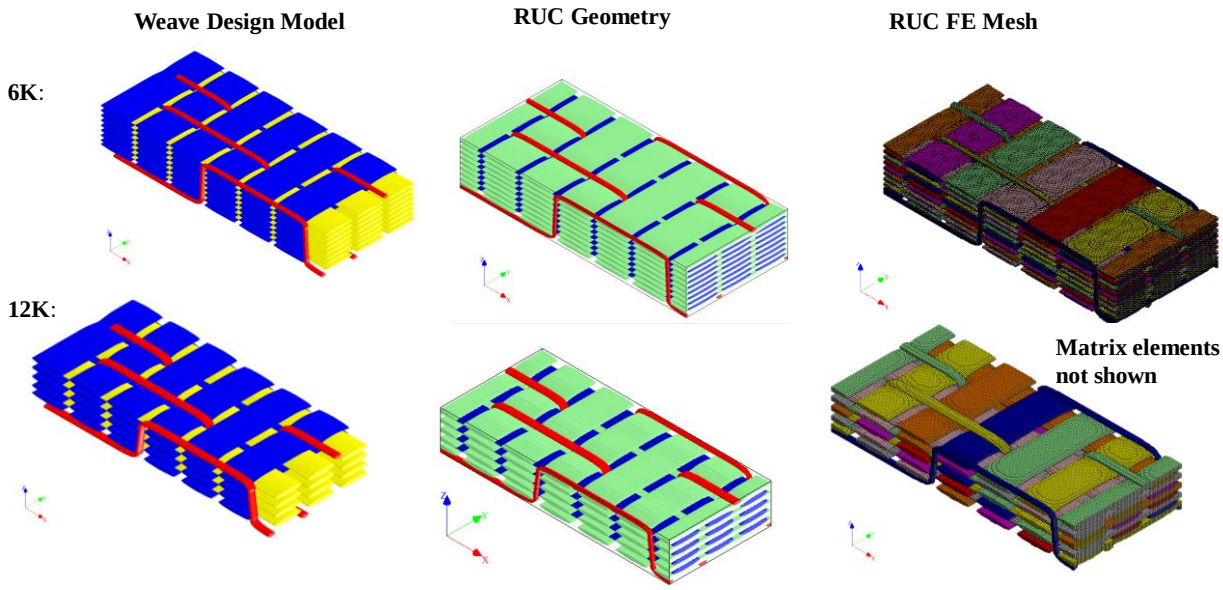

Figure 11. The weave design, geometry, and FE mesh for the AS4/RTM6 6K and 12K RUCs.

5.1.2 Multiscale Generalized Method of Cells (MSGMC)

The Generalized Method of Cells (GMC) micromechanics theory is an efficient, semi-analytical method that provides the homogenized, nonlinear constitutive response of composites. The GMC theory assumes a first-order displacement field in the subcells at a given scale, resulting in constant stresses and strains per subcell and has been extensively validated in the literature [5]. The GMC method considers the composite microstructure, on a given length scale, to be periodic, with an RUC as shown (at a given length scale) in Figure 12. The unit cell is discretized into a number of subcells, each of which may contain a distinct material. The MSGMC extends traditional single scale GMC analyses by allowing that the materials occupying the subcells on a given length scale may themselves be heterogeneous composite materials with their own unique RUC. A given analysis may consist of k arbitrary explicit length scales (see Figure 12). The highest length scale considered is denoted as Level 0, whereas, the current length scale under consideration is length scale i, where $i = 0, 1, \ldots, k$. In the MSGMC, the scales are linked by considering the RUC-averaged stress, strain, and stiffness tensors at scale i to be equal to the local subcell stress, strain, and stiffness tensors of the applicable subcell from the next higher length scale (i-1), including appropriate coordinate transformations. While this work is focused on determining effective elastic properties, the MSGMC can also perform multiscale localization of the stress and strain tensors (*i.e.*, determining stresses/strains in every subcell at each length scale). The reader is referred to Refs. [6, 7] for a detailed documentation of the MSGMC theory.

The MSGMC has recently been used to predict effective elastic properties of IM7/RTM6 3D orthogonal woven composites [6]. In order to develop a model of a 3D woven composite in MSGMC, a number of Matlab® scripts were developed to convert voxel-based finite element meshes into an appropriate RUC for an MSGMC analysis. A two-step homogenization procedure was used to determine the effective mechanical response for the composite by homogenizing

subcells in the thickness direction prior to homogenizing in-plane and is typically performed in MSGMC analyses of woven composites [6, 7].

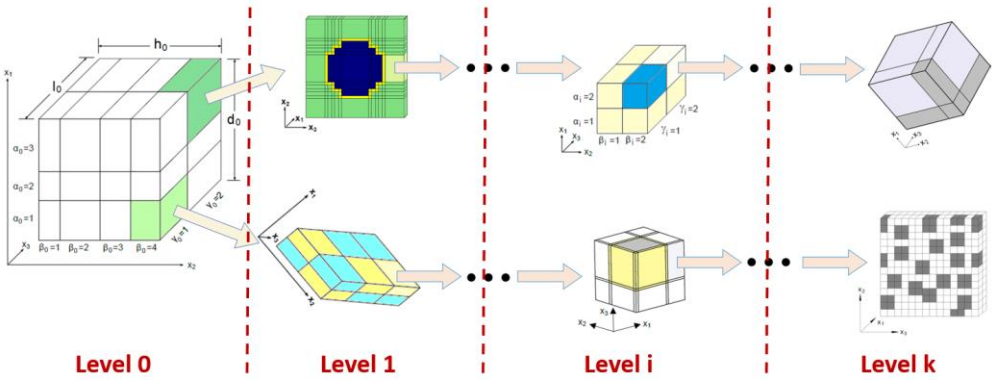

Figure 12. MSGMC RUCs and sub-cells across an arbitrary number of length scales.

This procedure required defining a number of "stacks" (*i.e.*, single columns of subcells in the thickness direction). An example of these stacks for a 3D orthogonal woven composite is shown in Figure 13. Within a stack, each sub-cell represents a section of warp, weft, and/or linker tows including its appropriate material orientation. In the MSGMC analysis, duplicate stacks were identified and removed from the model to reduce memory requirements. For comparison purposes, the same tow material properties were used as in the finite element simulations. Future work could include an additional lower length scale to model the behavior within each tow. Additionally, the MSGMC analyses in this study utilized the same discretization as the finite element analyses. However, converged elastic property estimates likely could have been obtained with a significantly coarser discretization. This topic is a subject of ongoing research.

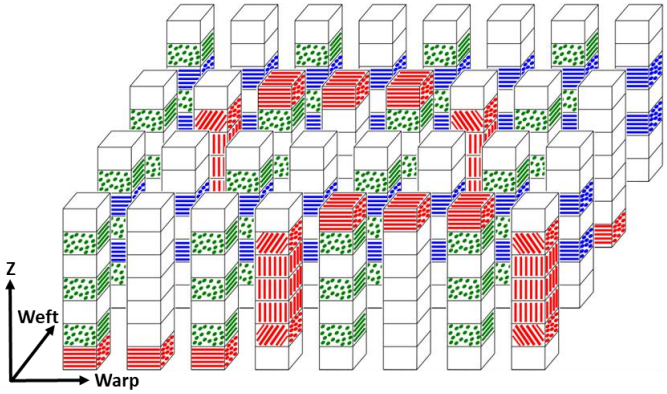

Figure 13. MSGMC 3D orthogonal woven representation.

5.2 Property computations and analysis results

Table 4 contains the calculated elastic constants, at RTA, for both the 6K and 12K weave architectures obtained from MSGMC and FE based analyses. All values are generally in good agreements with the largest difference that was reported for the v_{12} to be around 12%.

Table 4. Computed elastic properties for both weave architectures using MSGMC and FE-bases techniques.

Configuration	Method	Material Parameter/Property								
		E_{11} (GPa)	E_{22} (GPa)	E_{33} (GPa)	ν_{12}	ν_{13}	ν_{23}	G_{12} (GPa)	G_{13} (GPa)	G_{23} (GPa)
AS4 6K/ RTM6 (SN005)	**MSGMC**	**61.98**	**60.10**	**9.26**	0.059	0.444	0.446	3.39	2.25	2.26
	Digimat-FE	**61.83**	**59.91**	**9.69**	0.056	0.443	0.429	3.28	2.45	2.47
	% Δ	-0.2	-0.3	4.7	-5.1	-0.2	-3.8	-3.0	8.7	9.3
AS4 12K/ RTM6 (SN006)	**MSGMC**	**56.80**	**57.02**	**8.89**	0.059	0.444	0.449	3.21	2.14	2.18
	Digimat-FE	**56.40**	**57.50**	**9.31**	0.052	0.448	0.425	3.03	2.37	2.42
	% Δ	-0.7	0.8	4.8	-11.9	0.9	-5.3	-5.6	10.9	11.0

As for the comparison with the test data, the only available experimental data in these test series were E_{11}. The E_{11} obtained from analysis is relevant to be compared to tensile modulus in RTA (AP). The models and analyses did not account for any micro-cracks; however, for sake of comparison, the RTA (TC) data were also included in this evaluation. The results are indicated in Table 5 and also graphically shown in Figure 14.

Table 5. Analysis results as compared with elastic moduli obtained from different conditions and using different instrumentations.

Condition	Panel#	Strain Gage (from 5 Tests)				DIC (from 2 Tests)			
		E_{11} (GPa)	SD	% Δ to MSGMC	% Δ to Digimat-FE	E_{11} (GPa)	SD	% Δ to MSGMC	% Δ to Digimat-FE
RTA (AP)	SN005	57.6	3.3	7.5	7.3	57.1	0.2	8.6	8.4
	SN006	53.5	4.7	6.2	5.4	50	0.6	13.7	12.9
RTA (TC)	SN005	57.9	4	7	6.8	54.5	0.9	13.7	13.4
	SN006	48.1	3.4	18	17.2	48.2	0.4	17.9	17.1

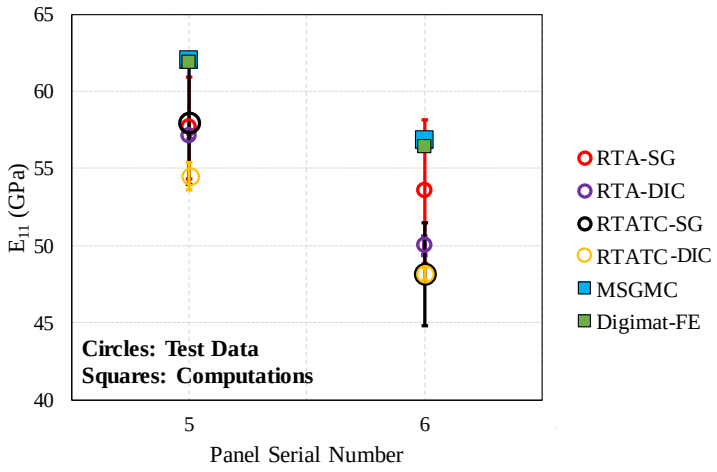

Figure 14. Graphical representation comparing analysis and test results, including test data standard deviations.

In general, analyses over-predicted the (averaged) test data. The amount of over-prediction, however, was a function of the instrument type used to measure strains in tests (See Table 5).

This amount was further higher when the analysis results were compared to TC test data. The sources for these differences can be thought as: i) the analyses did not account for micro-cracks in the materials; and ii) irregularities in the weave patterns (*e.g.*, varying yarn cross-sections and distorted yarns, etc.) could not be modeled and analyzed. In addition, the constituent materials' properties (AS4 fiber and RTM6 resin) obtained from literature and used in current analyses may not be accurately applicable due to batch-to-batch material property variations, differences in cure processes, etc. This topic is also a subject of ongoing research and more developments are expected as more test data become available and further trade studies are performed.

6. SUMMARY

In this study, eight panels were fabricated and subjected to materials characterization and mechanical testing. The 3D orthogonal weave architectures were composed of 6K and 12K yarn configurations infused with four different resin systems. Optical microscopy and X-Ray CT revealed the presence of micro-cracking in the as-received materials. The micro-cracking increased in all panels as the materials were subjected to thermal cycling. Overall, the thermal cycling and testing the materials at ETW environment did not significantly reduce the tensile performance of the panels in the warp direction. Analyses over-predicted the test results by ~5% to ~13% for the AP materials and these differences increased as the materials were subjected to thermal cycling as there were no means to account for such cracks in modeling and analysis.

7. ACKNOLEDGMENTS

X-Ray CT support provided by Grace Fischetti and Justin Jones from Materials Branch at NASA GSFC is greatly appreciated. Authors are also thankful for the 3D weave design and fabrication support provided by Mr. Hakan Gokce of BRM, Inc.

8. REFERENCES

1. Tsukrov, I., Bayraktar, H., Giovinazzo, M., Goering, J., Gross, T., Fruscello, M., Martinsson., L. "Finite element modeling to predict cure-induced microcracking in three-dimensional woven composites". *International Journal of Fracture* 172 (2011): 209-216.
2. Bayraktar, H., Tsukrov, I., Giovinazzo, M., Goering, J., Gross T., Fruscello, M., Martinsson, L. "Predicting cure-induced microcracking in 3d woven composites with realistic simulation technology". *Proceeding of International SAMPE Tech. Conf.* Baltimore, MD, May 21-24, 2012.
3. TexGen. Available from: http://texgen.sourceforge.net/index.php/Main_Page
4. Digimat, 2018. Available from: http://www.e-xstream.com/products/digimat/about-digimat.
5. Aboudi, J., S.M. Arnold, and B.A. Bednarcyk, *Micromechanics of composite materials*. Elsevier, Oxford, UK, 2012.
6. Ricks, T.M., B. Farrokh, B.A. Bednarcyk, and E.J. Pineda. "A comparison of different modeling strategies for predicting effective properties of 3D woven composites". *AIAA SciTech Forum*. 2019. San Diego, CA.
7. Bednarcyk, B.A. and S.M. Arnold, "Micromechanics-based modeling of woven polymer matrix composites". *AIAA Journal*, Vol. 41, No. 9, 2003, pp. 1788-1796. doi: 10.2514/2.7297.